

# HIGH VERTICAL RESOLUTION NUMERICAL SIMULATION OF SUMMER FLOWS IN CATALONIA. IMPLICATIONS TO SPATIAL AND TEMPORAL VARIABILITY OF OZONE AND PM10 LEVELS

M.R. Soler<sup>1</sup>, R. Arasa<sup>1</sup>, M. Merino<sup>1</sup>, M. Olid<sup>1</sup>, S. Ortega<sup>2</sup>

<sup>1</sup> Departament d'Astronomia i Meteorologia. Universitat de Barcelona, Barcelona, Spain.

<sup>2</sup> Departament de Física i Enginyeria Nuclear, Universitat Politècnica de Catalunya, Vilanova i la Geltrú, Spain

**Abstract:** The aim of this study is to analyze the dynamics of the sea-breeze and its effects on the 3D pollution transport using ground based monitoring station, Sodar measurements and numerical simulation. We use the non-hydrostatic atmospheric model MM5 coupled to the photochemical model CMAQ. Measurements are basically focused on the determination of the propagation of the sea breeze front inland and on the validation of the model outputs. Numerical simulation is useful not only to study the inland propagation, but also to analyze the thermal internal boundary layer, the head wind and all the interesting components of the sea breeze circulation phenomena, including the transport of pollutants inside it.

**Key words:** *Sea-breeze, numerical simulation, pollutant transport.*

## 1. INTRODUCTION

Sea-breeze phenomenon complexity gave rise to much interest in the understanding of the dynamics of the lower troposphere during sea-breeze events (Simpson 1994). More recently studies devoted to model and to predict pollutants dispersion under sea-breeze conditions point out the need to go deeper on the study of the dynamics of the sea-breeze structure using high resolution numerical simulations to resolve its fine scale, especially on the vertical direction.

In this study, we analyze a representative sea-breeze event in the Catalonia area, located in the northeast part of Spain. Catalonia is characterized by complex topography with Pyrenees in the northern part, a central depression, and the pre-littoral and littoral mountain ranges. To analyze sea-breeze, we use ground based instruments and the 3D non-hydrostatic atmospheric model MM5 (Grell et al. 1994) with 1-km horizontal resolution and high vertical resolution, where vertical grids included 45 levels up to 4.000 m a.g.l, with a first level at 8-m. Pollutants transport inside sea breeze and their redistribution is simulated by coupling MM5 model to the CMAQ photochemical model (Byun et al. 1999). Results show the meteorological model capability to identify the sea breeze structure using high vertical resolution, as well as to simulate the transport of pollution near the ground and and the distribution into higher layers.

## 2. EXPERIMENTAL SET-UP AND MODEL

### Ground based instruments.

We used a Doppler Sodar, a SCINTEC FAS64 (Phase array), deployed in la Plana area (Figure 1) from April 2000 to September 2001 (Soler et al., 2004). During this experiment data was obtained from 20 to 600 m with variable vertical resolution ranging from 20 m at the first levels to 60 m at the last ones. Measurements of the three wind components, its standard deviation and echo intensity were stored as 15 minutes mean values. In addition, we used in this study data from several meteorological ground stations placed in the studied area (Figure1) belonging to a surface stations network.

### Mesoscale modelling system

The mesoscale modelling system is composed by the PSU/NCAR mesoscale model, MM5 (Grell et al., 1994), version 3.7. Four domains 2-way nested are defined using the following resolution: 27, 9, 3 and 1 km. Initial and boundary conditions were updated every six hours with information obtained from the European Centre for Medium-Range Weather Forecast (ECMWF) model with a 0.5°x 0.5° resolution. For the two inner domains, we use a topography and land-use data base with 30" resolution. For the two outer domains the horizontal resolution was 5'. High vertical resolution is prescribed including 45 levels up to 4.000 m a.g.l with higher resolution (15 m approximately) at the lowest levels are considered. ETA parameterization was chosen for planetary boundary layer because it uses turbulent kinetic energy as a prognostic variable, which is a useful variable to detect the sea breeze front and the thermal internal boundary layer. For the land surface scheme, we activated the five-layer soil model, where temperature is predicted using the vertical diffusion equation for 0.01, 0.02, 0.04, 0.08, and 0.16 m deep layers from the surface with the assumption of fixed substrate. Solar radiation was parameterized by using the cloud-radiation scheme.

The photochemical model used in this study was the U.S.E.P.A CMAQ model (Byun et al., 1999) using CB05 chemical mechanism. Initial and boundary conditions were taken from a general profile.

### Ground –based monitoring and modelling the sea breeze

The simulation started at 0000UTC on June 20th 2000 and ended at 2400 UTC on June 22th 2000. In order to give a detailed description of the breeze's structure, the analysis was focused on June 21th 2000, preferably using results

from the smallest domain. The synoptic situation during this period, especially for the studied day, was anticyclonic with small pressure gradients favouring the development of mesoscale circulations such as the sea breeze.

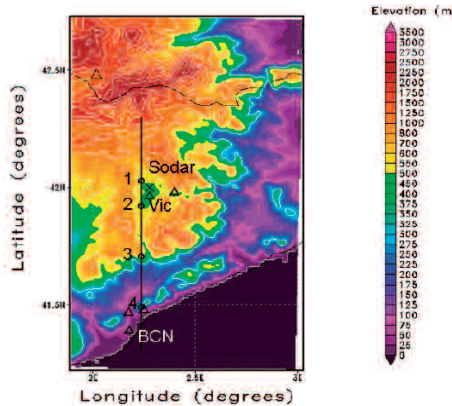


Figure 1. Geographic area of the smallest domain. Triangles represent the locations of the ground stations, cross symbol represents the position of the Sodar. Cross sections are taken along the solid line. Small circles are selected points named 1, 2, 3 and 4 referenced in the text to study the sea-breeze front characteristics.

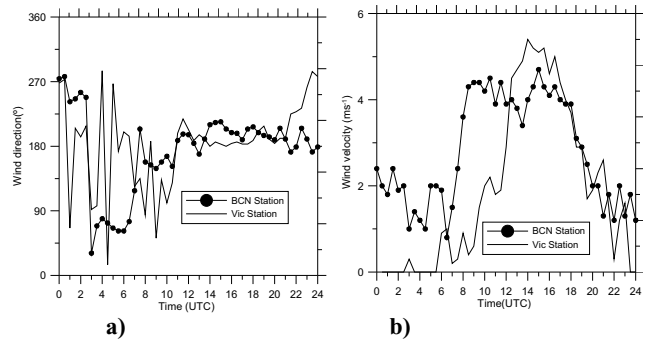


Figure 2. Temporal evolution of wind direction (a) and wind speed (b) at two stations: (BCN) located near the coast, and (Vic) located inland.

At BCN, in the early morning, wind direction veered from west to northeast while wind direction at Vic was continuously veering because wind velocity was near zero (Fig. 2b). At BCN, the sea-breeze onset was well detected early in the morning at 08 UTC by the change of wind direction from east to south sectors, setting up definitively at 11 UTC. At Vic, the sea-breeze onset was well detected later, at 12 UTC, setting up definitively at 14 UTC. The passage of the sea-breeze front was characterized by a significant increase in wind velocity (Fig. 2b), from 1 to 4.5  $\text{ms}^{-1}$  at BCN, and from 2 to 5  $\text{ms}^{-1}$  at Vic. Wind velocity decreases significantly, from 1700 UTC at Vic, and from 1800 UTC at BCN. At BCN, wind direction stayed being from the south direction, while at Vic station veered progressively to the west direction.

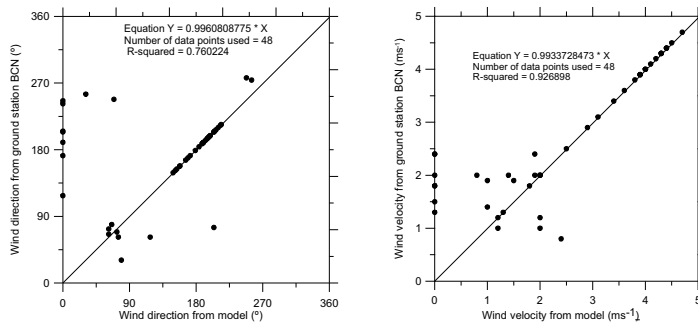


Figure 3a. Comparison for wind directions and wind speeds at BCN station.

Figure 3a shows the wind directions and speeds comparison between the model simulations and the observations at the representative meteorological station at BCN. The calculated wind velocities and directions are in good agreement with the observations, especially for high velocities and wind coming from the south sector corresponding to the sea-breeze. The agreement is worse for wind direction.

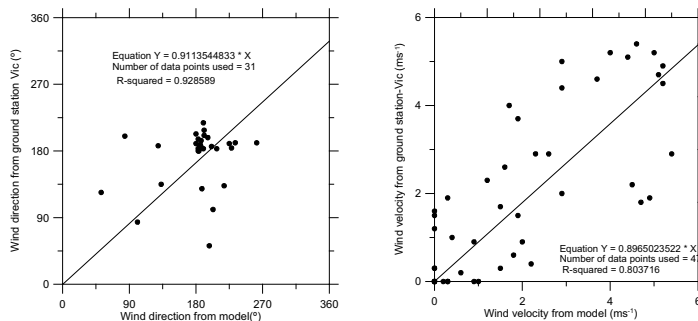


Figure 3b. Comparison for wind directions and wind speeds at Vic station.

Figure 3b shows the same comparison as figure 3a, but for Vic station. Wind direction comparison was made filtering wind velocities lower than  $0.5 \text{ ms}^{-1}$ , since the wind directions in these conditions were unreliable. Results for this station are in good agreement for wind direction comparison, especially those coming from south sector which corresponds to the sea-breeze. The correspondence is remarkably worse for wind velocity.

Horizontal maps for wind field at 10 m a.s.l are shown in figure 4. Vectors indicate wind direction while colour scale relates to wind speed magnitude. During night time, such as at 0300 UTC (left panel figure), wind is led by the complex topography of the studied area. During day time, such as at 1000 UTC (central panel), sea breeze begins to develop firstly near the coast indicating the sea breeze onset, while during the subsequent hours, such as at 1600 UTC (right panel), the sea breeze propagates further inland up to a distance of about 60 km. From this point is blocked up by the complex topography.

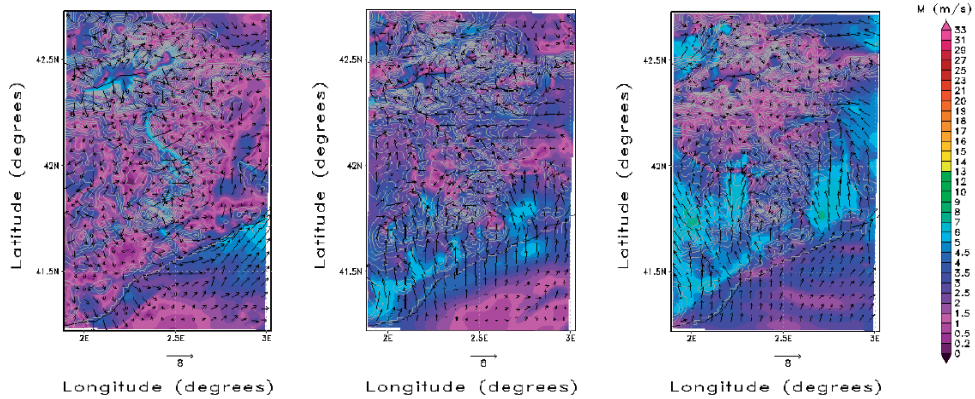


Figure 4. Development of sea-breeze is can be seen through the wind speed (colour scale) and velocity (vectors) at 10m agl at 0300 UTC (left panel), 1000 UTC (central panel) and 1600 UTC (right panel)

### 3. VERTICAL STRUCTURE OF THE ATMOSPHERIC BOUNDARY LAYER (ABL) DURING A SEA-BREEZE EPISODE.

In this section, we use basically the output analysis of the MM5 mesoscale model through a cross section in the south north direction (figure 1) in order to try to understand the sea-breeze system behaviour, its inherent stratification, and specially to obtain a detailed analysis of some of its components: the sea-breeze front, the associated gravity current, the development of Kelvin- Helmholtz billows, and the evolution of the thermal internal boundary layer. Moreover, a Sodar Doppler located in la Plana, near Vic station, helped us to monitor wind profiles.

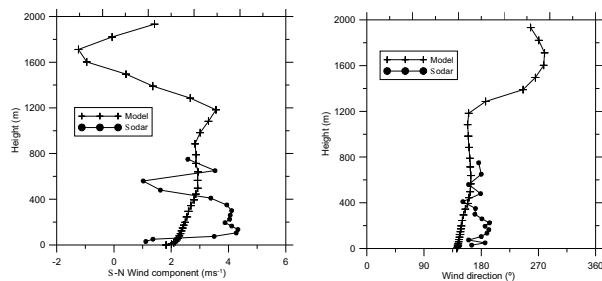


Figure 5. Comparison between vertical profiles of measured and modelled values for S-N wind components and wind direction.

#### Sea breeze characteristics using Sodar Doppler

The Sodar Doppler was located in “La Plana”, placed in a complex topographic area almost completely surrounded by mountains, with only two narrow corridors connecting it with neighbour areas. This configuration yields different flow patterns development, among them the sea-breeze which transport pollutants from the industrialized coastal area to La Plana leading air pollution problems. Sea-breeze analysis using Sodar measurements (Soler et al., 2004) showed its main characteristics: it starts approximately at 1300 UTC and develops during 8 hours approximately;

its return is above the vertical range of Sodar; and a maximum between  $5-6 \text{ ms}^{-1}$  is located at 150 m approximately. For this study, model results at Sodar location grid point were compared with Sodar measurements. Figure 5 presents the vertical profiles comparison between measured and modelled values of the S-N wind component and wind direction. Results show a good agreement for wind direction, but worse for the S-N component of the wind direction.

#### Sea-breeze front

Sea-breeze front is the landward edge of the sea-breeze flow, generally associated with a sudden variation of the wind direction, the wind speed, the moisture and the temperature. In addition, the meeting of marine and continental air masses induce thermal and mechanical turbulence that the model must detect as an increment of turbulent kinetic energy and high fluctuations of vertical wind velocities with updrafts within continental and marine air masses in the vicinity of the sea breeze front. Sea breeze front circulation is characterized by analyzing the modelled vertical profiles of these previous magnitudes over points 1, 2, 3 and 4 located along the solid line of Figure 1.

Profiles of wind direction indicate the sea breeze front onset. At point 1, located near the coast, the sea breeze arrives at 0800 UTC as the direction change abruptly from west sector to southeast sector, at point 2 the sea breeze front

arrives at 0940 UTC with analogous characteristics. At point 3 arrives at 1100 UTC veering from east to south sector, while at point 4 the arrival is later, at 1340 UTC, in this case the model indicates winds veering from east to southeast direction.

The spatial distributions of potential temperature and TKE reveal the changes in the coastal and inland atmospheric boundary layer due to sea breeze occurrence, because the stability structure of the boundary layer is altered when air from a cold-water surface passes over a warmer land surface. An adjustment also occurs in the advecting air according to the change in the surface roughness. These alterations lead to the formation of a TIBL, which vertical growth depends on the convective and mechanical turbulence. It is a shallow unstable layer with a neutral or stable layer aloft. When TIBL forms, it limits the vertical spread of pollutants and the fumigation phenomena can be held inside the TIBL in coastal regions as we will see in next section. In this section, its horizontal and vertical structure is examined from the vertical profiles simulated along the cross section. The simulated potential temperature profile after the sea breeze onset at the coast (point 1) indicates the formation of a TIBL which vertical extent is about 250m (figure 6a) from the base of the lowest inversion in temperature profiles. The TIBL increase with inland distance, which gradually merges with the generic inland boundary layer, as seen from the potential temperature profiles at points 2, 3 and 4 (figure 6a). In addition, TKE vertical profiles also give a measure of the vertical extent of the coastal and inland PBL, as seen in figure 6b. It is important to remark the TKE second peak value appearing at point 3 at 1120 UTC, prevailing from near 11 UTC (time of the sea breeze arrival) until 13 UTC. It is known the occurrence of coherent structures, such as Kelvin Helmholtz billows close to the sea breeze front, particularly within the elevated head region and also between the sea-breeze flow itself and the return flow aloft. Under strong shear and static stability, Kelvin Helmholtz billows development occur: the billows grow, reach maturity and eventually break as they propagate backwards away from the front and are centred along the zero-velocity boundary separating the sea-breeze and the return current. The associated mixing is known to have important consequences for the inland propagation and for pollutant dispersion.

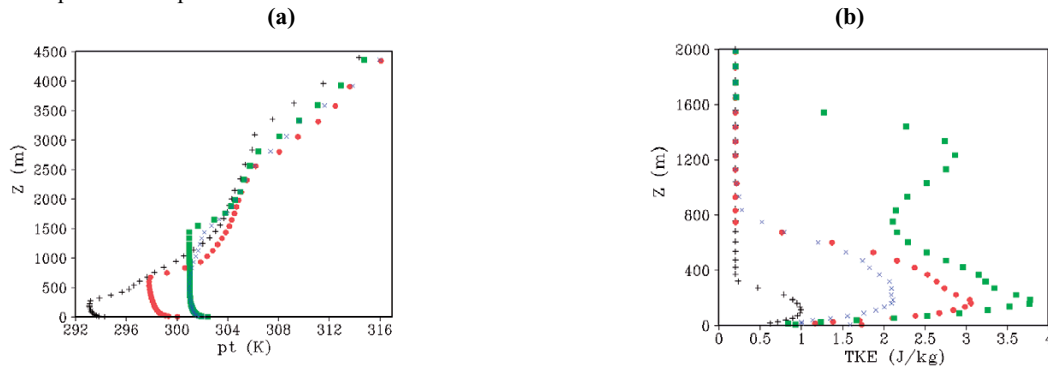


Figure 6. Vertical profiles for simulated potential temperature (a) and turbulent kinetic energy (b). At points: (1) in black at 0800UTC; point (2) in red at 1300 UTC; point (3) in green at 1120 UTC; and point 4 in blue at time 14 UTC.

#### 4. DISTRIBUTION OF POLLUTANTS UNDER SEA-BREEZE CONDITIONS

In order to study the 3D distribution of ozone and particles under sea-breeze conditions, MM5 model was coupled to the photochemical model CMAQ. The pollutants were emitted continuously, from 00UTC to 2400 UTC, from one source located at ground level in one of the industrial areas of Barcelona near the coast (see Fig. 7a). That source emits  $\text{NO}_2$ , VOC's, and PM10 with a chosen emission rate of 192, 39,5 and  $72 \text{ gs}^{-1}$  respectively. Here we will only comment the particles distribution, since ozone one has similar characteristics, even though this presents some peculiarities which would need a deeper study. Figure 7a and 7b present the resulting concentrations of PM10 in ( $\mu\text{gm}^{-3}$ ), simulated by the model in two horizontal sections at 14 UTC: at ground level (Fig. 7a) and at 400m (Fig. 7b). At ground level, we can clearly see the sea-breeze transporting the plume particles inland and the location of the front. The second maximum located on the right side of the plume is a consequence of the plume dispersion during night time. During this time the horizontal wind comes from the west-southwest sector (see Fig. 4a). Therefore, the maximum concentration is located over the sea, parallel to the coast line. From sea-breeze onset, these particles are transported inland as we can see in Figure 7a. Figure 7b shows a clear example of fumigation. As we have seen in last section, the sea breeze onset reduces abruptly the mixing layer depth to the TIBL depth, which is approximately 250m near the coast. In these conditions, particles are trapped inside the TIBL. Therefore, the concentration near the coast but at levels higher than TIBL depth is near zero. In addition, the gravity current carries them horizontally inland, up to the sea breeze front, where they are carried up and mixed. Figure 8 illustrates the PM 10 concentration vertical distribution at 14 UTC along the South-North line. Once the PM10 are transported in altitude by the sea-breeze front, they are distributed seaward by the headwind located in altitude at the top, and behind the sea breeze front.

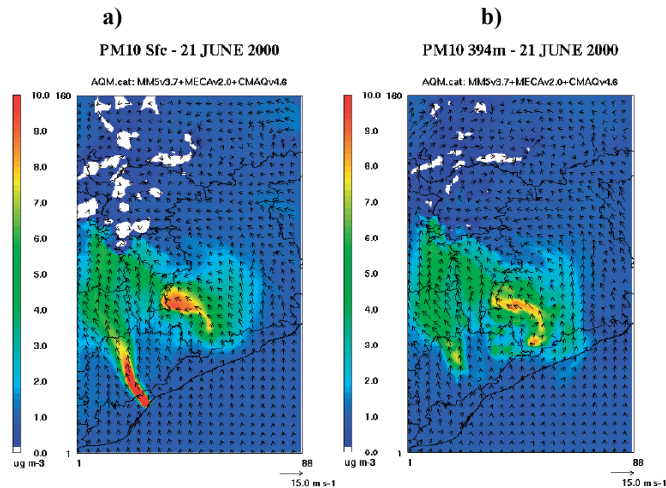


Figure 7. Horizontal cross section at 1400 UTC for the PM10 concentration in  $\mu\text{g m}^{-3}$  (colour scale) simulated by CMAQ model and horizontal wind velocity (vectors) simulated by the MM5 model: a) at 10 m above ground level and b) at 394 m above ground level.

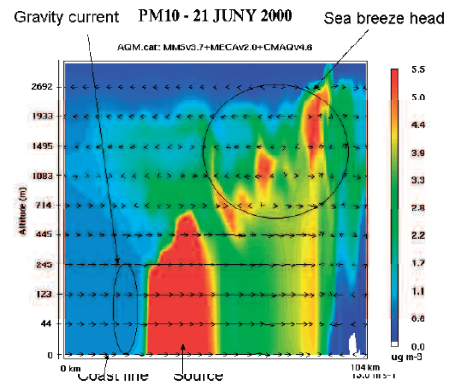


Figure 8. North-South vertical cross section for PM10 concentrations in  $\mu\text{g m}^{-3}$  (colour scale) simulated by the model, with the wind velocity (vectors) at 1400 UTC.

## 5. CONCLUSIONS

In this study, the structure of the boundary layer during a sea-breeze event has been analyzed using numerical simulations and some ground based measurements. The modelled sea-breeze entrance is in quite good agreement with observations. Likewise, the model reproduces quite well the TIBL behaviour. As the sea breeze penetrates inland, vertical ascent of air occurs at sea-breeze leading front and subsidence at the rear side of it. These cause the ABL top to slope downwards from land to sea. As a result, the height of the TIBL near the coast is only 250 m, leading to the phenomena of fumigation. Pollutants emitted inside the sea-breeze area are transported in altitude by the sea-breeze front and distributed seaward by the head wind in altitude, leading to an elevated reservoir of pollutants which could be incorporated to the next sea-breeze system.

## REFERENCES

- Byung, D.W. and J.K.S. Ching, Eds., 1999: Science algorithms of the EPA Models-3 Community Multiscale Air Quality (CMAQ) Modelling System EPA-600/R-99/030, Office of Research and Development, U.S. Environmental Protection Agency, Washington D.C.
- Grell, G.A., J. Dudhia and D.R. Stauffer, 1994: A description of the fifth-generation Penn State/NCAR mesoscale model (MM5). *NCAR Tech. Note, NCAR/TN-398+STR*, 117 pp.
- Simpson, J.E., 1994: *Sea breeze and Local Wind*. Cambridge University Press. Cambridge, UK, 234 pp.
- Soler, M.R., J. Hinojosa, M. Bravo, D. Pino and J. Vilà Guerau de Arellano, 2004: Analyzing the basic features of different complex terrain flows by means a Doppler SODAR and a numerical model: Some implications for air pollution problems. *Meteorol. Atmos. Phys.*, **85**, 141-154.